Scientific Papers Series Management, Economic Engineering in Agriculture and Rural Development
Vol. 23, Issue 4, 2023
PRINT ISSN 2284-7995, E-ISSN 2285-3952

TECHNIQUES BASED ON UAV IMAGES FOR WHEAT PRODUCTION ESTIMATION

Ciprian BUZNA[1], Marinel Nicolae HORABLAGA[1,2], Florin SALA[1,2]

[1]Agricultural Research and Development Station (ARSD) Lovrin, Lovrin, 307250, Romania, E-mails: buznac@yahoo.com; hnm75@yahoo.com; florin_sala@usvt.ro
[2]University of Life Sciences "King Michael I" from Timisoara, Timișoara, 300645, Romania Emails: hnm75@yahoo.com; florin_sala@usvt.ro

Corresponding author: florin_sala@usvt.ro

Abstract

The aim of the study was to use a technique based on aerial images (UAV) to wheat production estimation. The images were taken with the drone (UAV, DJI Phantom 4) at different image capture heights (ICH), in the range of 1.5 - 50 m from the ground level, and resulted in 18 sets of images (trials, T). The resized images (crop image, 1,000 x 2,000 pixels) were analyzed and the information for RGB color parameters was obtained. Very strong correlations were recorded between color parameters R and G (r=0.993), as well as between these two color parameters and ICH (r=0.940 in the case of R, respectively r=0.918 in the case of G). Based on the trials distribution in the PCA diagram and in the CA dendrogram, 14 trials (T1, T3-T6, T8-T10, T12-T14, T16-T18) were selected for Training & model construction (Tmc), and four trials (T2 , T7, T11 and T15) for were used for Testing & model validation (Tmv). Through the regression analysis, a wheat production estimation model was obtained based on RGB parameters under statistical safety conditions (R^2=0.999, p<0.001). Flowchart diagram of process was proposed for the present study, and the work process, respectively the obtained models can be adapted for various other agricultural crops.

Key words: *Flowchart diagram, model, UAV image, wheat crop, yield prediction*

INTRODUCTION

Techniques based on imaging analysis have penetrated more and more into agricultural practices, and the facilities offered by these techniques are successfully used for the management of the farm, land and agricultural crops [2, 14, 21, 24].
Unmanned aerial vehicles (UAVs) have already been used for more than a decade in different approaches of general or specific aspects in agriculture, and facilitate studies and decisions in the optimization of technologies and productions for different crops [22, 27].
UAV-based techniques have been used in the study of land surfaces and modeling of different land categories [7], land administration [28], classification and phenotyping of agricultural crops [4, 29].
In the case of cereal crops, drones were used for observations, collecting images and data for the purpose of evaluating the state of the crops, characterizing different genotypes, and substantiating decisions to optimize yields [5, 20].
In the case of wheat crops, UAVs were used to evaluate some growth parameters and the status of wheat plants [9, 32], the evaluation of some foliar and physiological indices in wheat plants [34], plants nutritional status assessment [11], plants relationship with the water regime and the diagnosis of water stress in wheat [11, 37], wheat lodging [35], wheat biomass [15], wheat yield prediction [36], prediction of production variability and some wheat quality indices [38]. The use of UAVs in the study of crops presents a series of advantages, such as affordable costs, high image resolution, ease of use and flexibility of movement, which has made their popularity grow in agricultural practice [1, 19].
The present study used imaging analysis techniques, based on aerial images (UAV) in order to formulate a process flowchart diagram and production prediction models for the wheat crop, based on the spectral information from the captured digital images.

MATERIALS AND METHODS

The study was carried out at the Agricultural Research and Development Station Lovrin (ARSD), Timis County, Romania. The wheat crop, 'Dacic' cultivar, was taken into account in the present study.

Wheat crop was carried out on plot 4-7 Lovrin, on a chernozem type soil, in non-irrigated conditions, agricultural year 2021-2022.

The crop technology ensured disking soil tillage, sowing at the optimal time (Dacic wheat cultivar, seed of the superior biological category), mineral fertilization before sowing and in vegetation (NPK complex fertilizers, ammonium nitrate), foliar fertilization in vegetation (Naturamin), post-emergence weed control (Sekator, Falcon Pro), phytosanitary treatments.

A DJI Phantom 4 drone was used to take the images. The images were captured at different heights (ICH), from 1.5 m to 50 m above ground level.

Identical camera settings (FC330 camera model) were used for image acquisition. The images were taken at physiological maturity, BBCH code 9, Senescence [17]. Digital images were taken at 18 different heights in the specified range (1.5 to 50 m), Figure 1.

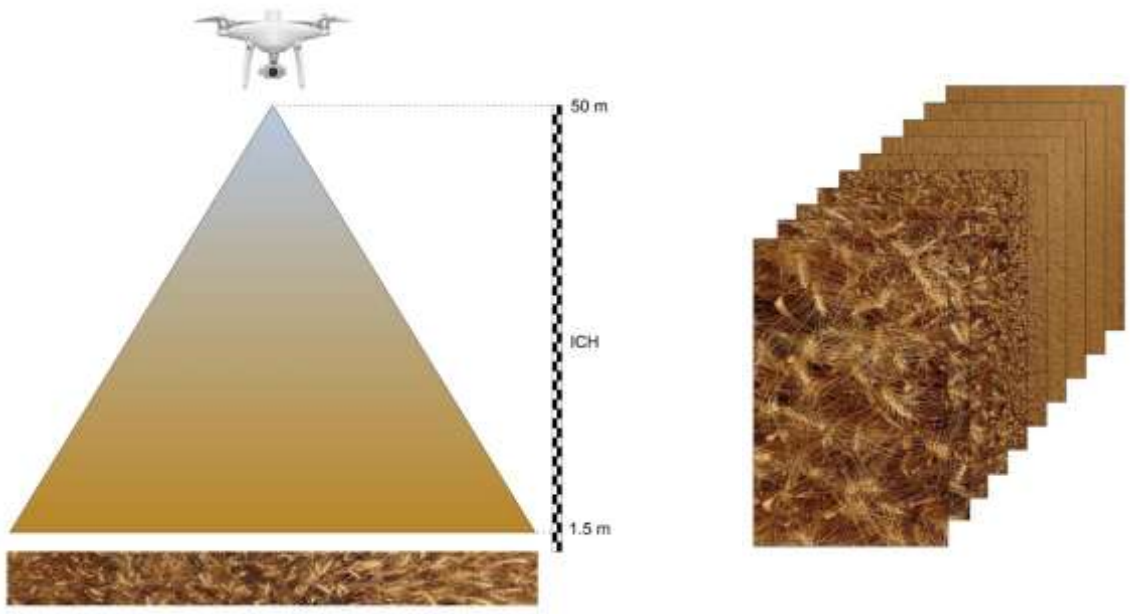

(a) (b)

Fig. 1. Aspects of image capture in wheat culture; (a) DJI Phantom 4 drone and image capture height (ICH); (b) selective presentation from the set of 18 images, relative to ICH
Source: Original figure, photos and concept of the authors.

The crop was mechanically harvesting, and the average production recorded, under the conditions of the 2021-2022 agricultural years, was 5,026 kg ha^{-1}. The images were processed by resizing (crop size, central area) in order to select a unitary area for analysis, with 1,000 x 2,000 pixels dimensions. The images were analyzed to obtain the spectral data, the RGB color system [23].

The data recorded by the study were analyzed by the ANOVA test, as well as by other appropriate statistical methods to quantify the relationship between the spectral values obtained from the aerial images (UAV), the images capture height, and production.

Based on PCA (Principal Component Analysis) and CA (Cluster Analysis), a number of 14 variants (T1, T3-T6, T8-T10, T12-T14, T16-T18) were selected for Training & model construction (Tmc) , and 4 other variants (T2, T7, T11 and T15) that were used for Testing & model validation (Tmv). Flowchart diagram concept of process used for this study is presented in Figure 2.

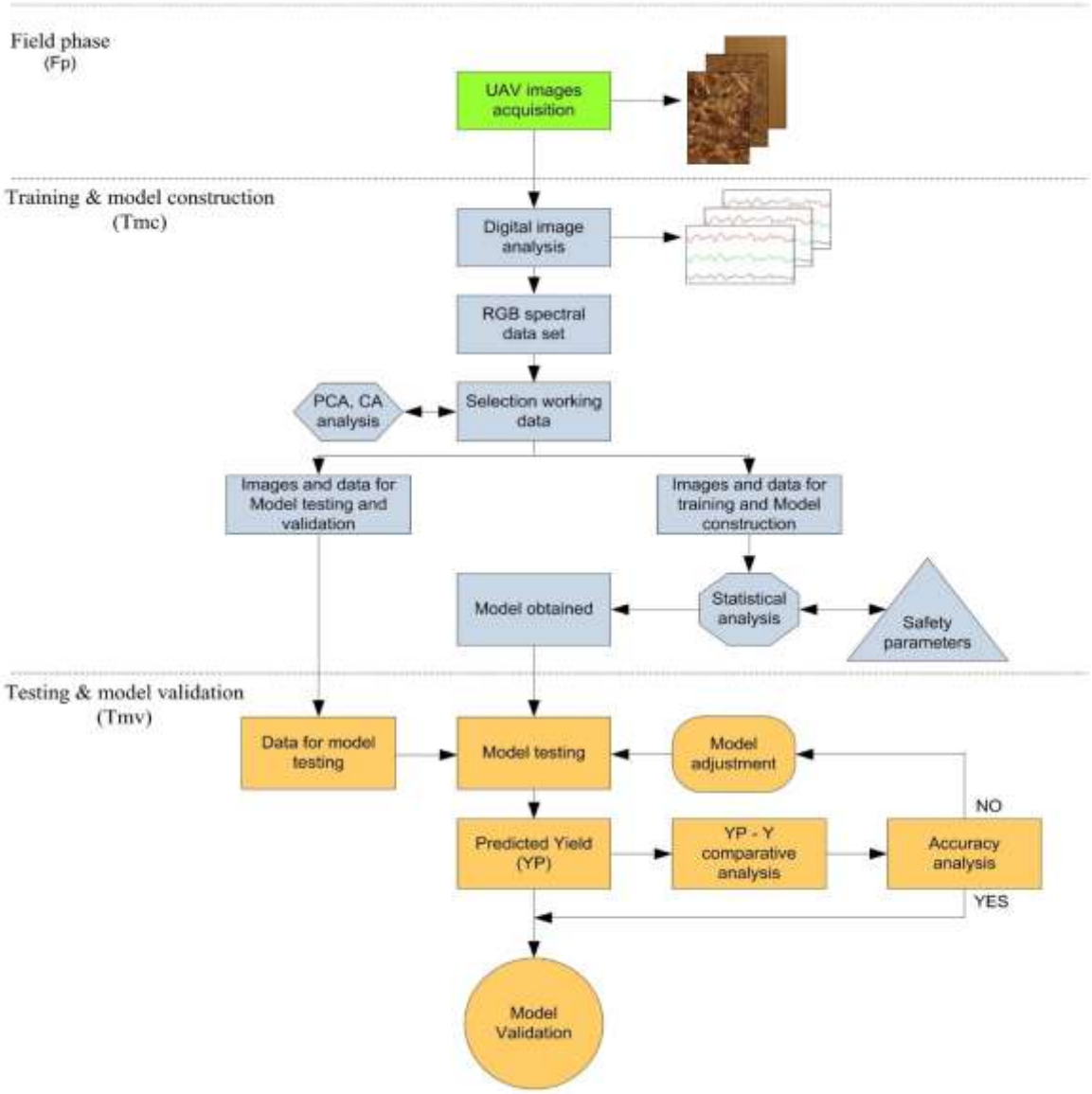

Fig. 2. Flowchart diagram of process used for this study
Source: Original figure, concept of the authors.

To confirm the safety of the data analysis and the results obtained, various appropriate statistical parameters were used; correlation and regression coefficients r, R^2; p parameter; RMSEP, equation (1), REP; and the Cophenetic coefficient.

$$RMSEP = \sqrt{\frac{1}{n}\sum_{j=1}^{n}\left(y_j - \hat{y}_j\right)^2} \quad (1)$$

Data analysis and processing was done with the EXCEL calculation module, Microsoft Office, and PAST [8, 10, 33].

RESULTS AND DISCUSSIONS

From the analysis of the digital images captured on the 18 height positions, relative to the ground level, the RGB spectral values were obtained. From the set of retrieved images, in the range of 1.5 - 50 m height (ICH), two categories of images use were established, respectively 14 images were used for Training & model construction (Tmc), and 4 images were used for Testing and model validation (Tmv).

Table 1 shows the variants (T1 to T18) in relation to the image capture height (ICH, m), the categories of images use (Tmc, Tmv), the RGB spectral values, and the calculated values for the standard error (SE).

Table 1. The RGB spectral values for the wheat crop, in relation to the images capture height, 'Dacic' cultivar

Trial	Images usage category	ICH (m)	Spectral data		
			R	G	B
T1	Tmc	1.5	132.4	87.68	48.13
T2	Tmv	2	127.29	80.83	42.94
T3	Tmc	3	123.25	77.11	40.2
T4	Tmc	4	124.6	78.9	41.04
T5	Tmc	5	123.74	78.53	39.94
T6	Tmc	6	126.04	81.14	41.56
T7	Tmv	7	125.13	80.67	41.42
T8	Tmc	8	127.62	82.85	42.32
T9	Tmc	9	126.86	79.19	36.33
T10	Tmc	10	128.19	80.32	36.56
T11	Tmv	15	133.79	88.94	45.36
T12	Tmc	20	136.53	91.96	47.18
T13	Tmc	25	141.09	95.7	47.86
T14	Tmc	30	144.15	98.88	50.08
T15	Tmv	35	144.56	98.65	48.19
T16	Tmc	40	145.38	99.21	47.81
T17	Tmc	45	145.88	99.26	47.1
T18	Tmc	50	146.59	99.95	47.45
SE			±2.08	±2.06	±0.99

Note: Tmc - Training & model construction; Tmv - Testing & model validation
Source: Original data from images analysis.

The ANOVA test, single factor, was used to analyze and evaluate the recorded data, under the aspect of statistical safety and the presence of the variance, and the results obtained are presented in Table 2 ($p<0.001$, $F=435.2939$, Alpha=0.001).

Table 2. ANOVA test

Source of Variation	SS	df	MS	F	P-value	F crit
Between Groups	139993.7	3	46664.58	435.293	2.67E-44	6.0766
Within Groups	7289.768	68	107.203			
Total	147283.5	71				

Source: Original data, obtained by calculation.

Based on the coefficient of variation (CV), it was assessed that high variability was recorded in the case of the G color parameter (CV_G=9.9960), intermediate values were recorded in the case of the B color parameter (CV_B=9.6311), and low variability of recorded in the case of the R color parameter (CV_R=6.6009).

The correlation analysis highlighted very strong and strong, positive correlations between the values of the color parameters (RGB) and in relation to the image capture height (ICH), under statistical safety conditions ($^{**}p < 0.01$, $^{***}p < 0.001$), Table 3.

Table 3. Correlation table

Variable		ICH	R	G	B
1. ICH	Pearson's r	—			
	p-value	—			
2. R	Pearson's r	0.940***	—		
	p-value	< .001	—		
3. G	Pearson's r	0.918***	0.993***	—	
	p-value	< .001	< .001	—	
4. B	Pearson's r	0.654**	0.830***	0.879***	—
	p-value	0.003	< .001	< .001	—

Source: Original data, obtained by calculation.

The regression analysis described the variation of the color parameters G in relation to R, equation (2), under statistical safety conditions (R^2=0.989, $p<0.001$), Figure 3.

$$G = -0.001622\,x^3 + 0.6483\,x^2 - 85.19\,x + 3{,}767 \quad (2)$$

where:
x – R, the values of the R color parameter

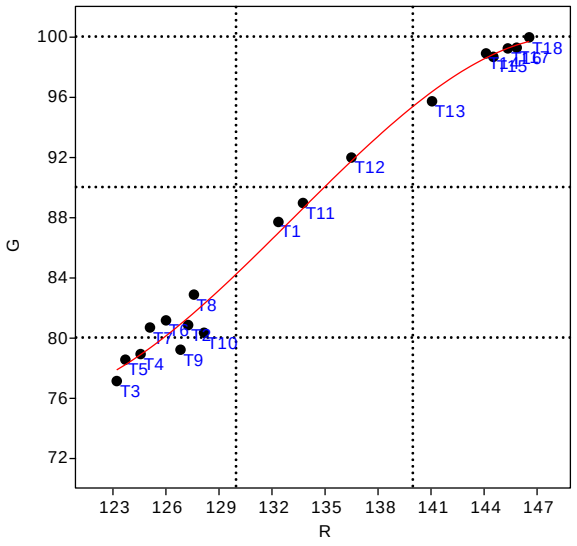

Fig. 3. Graphical distribution of G values in relation to R
Source: Original figure, based on data obtained.

The variation of the R and G color parameters in relation to the image capture height (ICH)

was described by degree 2 polynomial equations, equations (3) and (4), under statistical safety conditions (R^2=0.900, p<0.001, F=67.878 for R color parameter; R^2=0.867, p<0.001, F=49.18 for G color parameter). In the case of B color parameter, the statistical safety was low, R^2=0.445, p<0.05, F=6.0215.

The graphic models of the R and G parameters variation in relation to ICH are shown in Figure 4 (a) and (b).

$$R = -0.006101\,x^2 + 0.807\,x + 122.7 \quad (3)$$

$$G = -0.007447\,x^2 + 0.8563\,x + 76.85 \quad (4)$$

where:

x – ICH, image capture images (m)

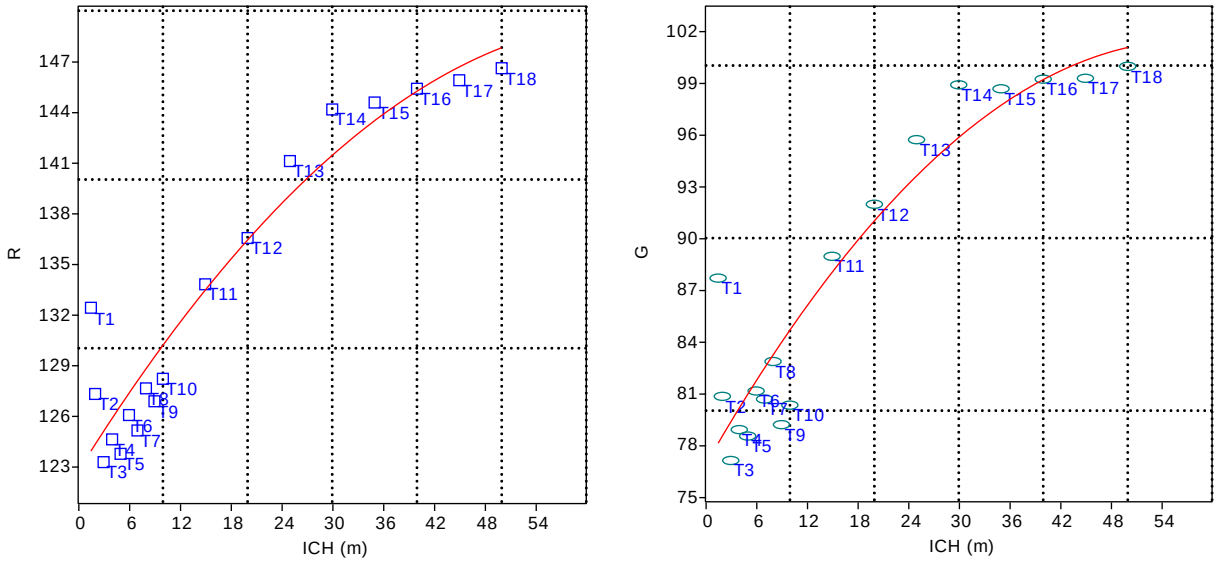

(a) (b)

Fig. 4. The graphic distribution of R (a) and G (b) values in relation to the image capture height (ICH) in the wheat crop, 'Dacic' cultivar

Source: Original figures based on recorded data

According to PCA, correlation, the diagram presented in Figure 5 was obtained. The distribution of the trials (T1 to T18) was found in relation to the affinity to the RGB color parameter, as biplot. PC1 confirmed 93.431% of variance, and PC2 confirmed 6.4967% of variance.

The trials distribution was the basis for selecting some variants for Training & model construction (Tmc) and other variants for Testing & model validation (Tmv).

Cluster analysis (CA) was used to find out the grouping of the trials, based on Euclidean distances, according to the degree of similarity in relation to the RGB values obtained at the 18 cases of images capture heights.

The dendrogram from Figure 6 was obtained, under statistical safety conditions (Coph corr. = 0.865).

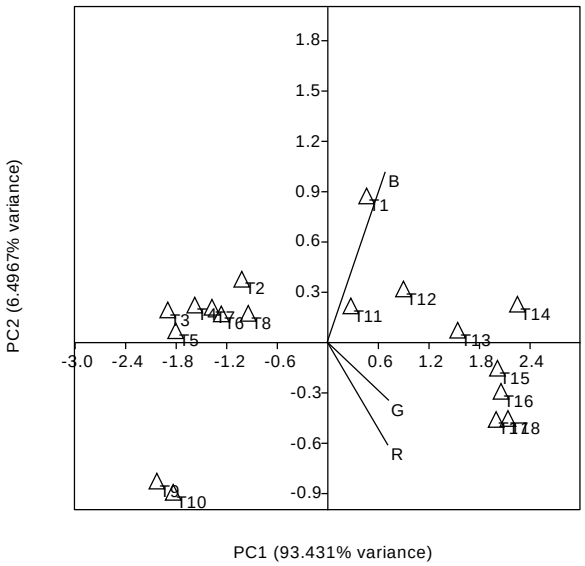

Fig. 5. PCA, correlation diagram

Source: Original figure based on recorded data.

The formation of two distinct clusters (C1 and C2) was found, and within each cluster there

are several sub-clusters. The grouping of the trials based on similarity, in relation to the RGB color parameter, was the basis for selecting some trials for Training & model construction (Tmc) and other trials for Testing & model validation (Tmv).

To confirm the level of similarity, the SDI values were calculated, in relation to which the highest level of similarity was found between T16 and T17 trials (SDI=0.870), followed by trials T6 and T7 (SDI=1.034), trials T17 and T18 (SDI=1.050) respectively for the T15 and T16 trials (SDI=1.063). The set of SDI values for all studied variants (T1 to T18) is presented in Table 4.

The regression analysis facilitated the obtaining of some equations that described the production in relation to the spectral values resulting from the analysis of the digital images, captured at different heights (ICH).

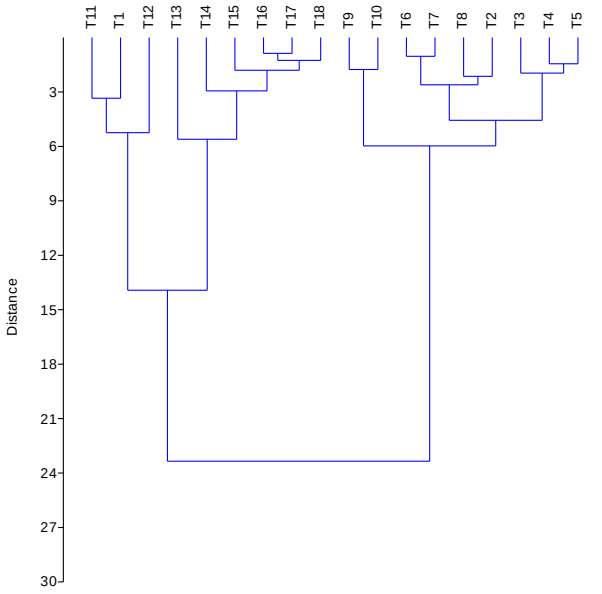

Fig. 6. Dendrogram of trials grouping based on Euclidean distances, in relation to RGB parameter values, 'Dacic' wheat cultivar
Source: Original figure based on recorded data.

Table 4. SDI values in the case of trials in relation to ICH, and RGB color parameters, UAV images, 'Dacic' wheat cultivar

	T1	T2	T3	T4	T5	T6	T7	T8	T9	T10	T11	T12	T13	T14	T15	T16	T17	T18
T1		9.999	16.073	13.718	15.02	11.24	12.12	8.941	15.55	14.34	3.346	6.023	11.82	16.34	16.37	17.36	17.80	18.77
T2	9.999		6.137	3.817	5.186	1.888	2.646	2.139	6.824	6.463	10.67	15.07	20.87	25.71	25.36	26.24	26.50	27.53
T3	16.073	6.137		2.394	1.525	5.087	4.207	7.519	5.686	6.925	16.66	21.10	26.88	31.75	31.33	32.18	32.40	33.45
T4	13.718	3.817	2.394		1.445	2.713	1.886	5.134	5.232	5.914	14.28	18.72	24.50	29.37	28.97	29.83	30.06	31.10
T5	15.026	5.186	1.525	1.445		3.838	2.950	6.275	4.817	5.868	15.45	19.90	25.66	30.55	30.10	30.95	31.16	32.20
T6	11.242	1.888	5.087	2.713	3.838		1.034	2.449	5.642	5.504	11.63	16.08	21.86	26.74	26.33	27.19	27.43	28.47
T7	12.125	2.646	4.207	1.886	2.950	1.034		3.430	5.576	5.754	12.60	17.04	22.84	27.71	27.32	28.18	28.43	29.47
T8	8.941	2.139	7.519	5.134	6.275	2.449	3.430		7.061	6.317	9.187	13.63	19.42	24.29	23.89	24.76	25.01	26.05
T9	15.557	6.824	5.686	5.232	4.817	5.642	5.576	7.061		1.760	14.98	19.34	24.65	29.59	28.85	29.59	29.67	30.72
T10	14.344	6.463	6.925	5.914	5.868	5.504	5.754	6.317	1.760		13.53	17.82	23.03	27.96	27.18	27.90	27.97	29.02
T11	3.346	10.671	16.663	14.280	15.45	11.63	12.60	9.187	14.98	13.53		4.466	10.25	15.11	14.77	15.67	15.99	17.01
T12	6.023	15.074	21.109	18.724	19.90	16.08	17.04	13.63	19.34	17.82	4.466		5.937	10.69	10.50	11.45	11.86	12.85
T13	11.828	20.875	26.880	24.509	25.66	21.86	22.84	19.42	24.65	23.03	10.25	5.937		4.940	4.566	5.543	6.016	6.963
T14	16.349	25.711	31.755	29.379	30.55	26.74	27.71	24.29	29.59	27.96	15.11	10.69	4.940		1.948	2.603	3.467	3.744
T15	16.377	25.365	31.336	28.976	30.10	26.33	27.32	23.89	28.85	27.18	14.77	10.50	4.566	1.948		1.063	1.817	2.522
T16	17.364	26.245	32.188	29.835	30.95	27.19	28.18	24.76	29.59	27.90	15.67	11.45	5.543	2.603	1.063		0.870	1.463
T17	17.801	26.506	32.409	30.068	31.16	27.43	28.43	25.01	29.67	27.97	15.99	11.86	6.016	3.467	1.817	0.870		1.050
T18	18.772	27.539	33.451	31.109	32.20	28.47	29.47	26.05	30.72	29.02	17.01	12.85	6.963	3.744	2.522	1.463	1.050	

Source: Original data, obtained by calculation.

Thus, Y production was described in relation to R and G values based on equation (5) under general statistical safety conditions, R^2=0.999, p<0.001, RMSEP=1.5526, REP=0.03. Based on the ANOVA test, the level of statistical confidence was found for all the coefficients of equation (5), p<0.001. Based on equation (5), a 3D model of production expression (Y) in relation to R and G was obtained, Figure 7, and a model in the form of isoquants, Figure

8. For high precision, up to 16 decimals for the equation (5) coefficients were used.

$$Y_{(R,G)} = ax^2 + by^2 + cx + dy + exy + f \quad (5)$$

where:

$Y_{(R,G)}$ – wheat production in relation to R and G; x – R spectral values; y – G spectral values; a, b, c, d, e, f – coefficients of the equation (5); a = -2.09485773; b = -2.04843713; c = 200.37349341; d = -191.04807646; e = 4.11077817; f = 0

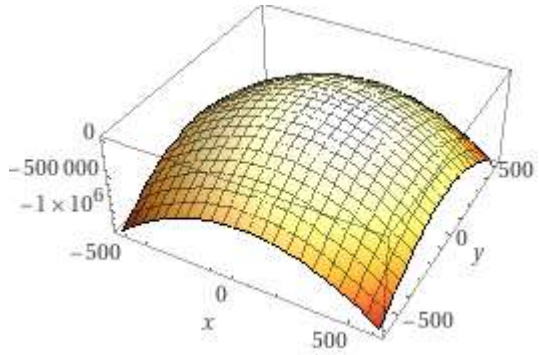

Fig. 7. The 3D graphic distribution of production (Y) in relation to the spectral values R (x-axis) and G (y-axis), Dacic cultivar
Source: Original graph based on recorded and calculated data.

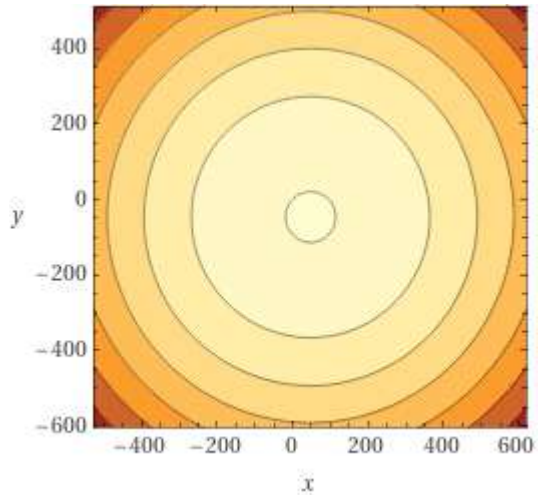

Fig. 8. The graphical distribution in the form of isoquants of the production (Y) in relation to the spectral values R (x-axis) and G (y-axis), Dacic cultivar
Source: Original graph based on recorded and calculated data.

Equation (6) described the Y production in relation to the R and B values in general statistical safety conditions, R^2=0.999, p<0.001, RMSEP=9.6026, REP=0.19. Based on the ANOVA test, the level of statistical safety for the coefficients x and x^2 of the equation (6) was found, p<0.001. Based on equation (6), a 3D model of production expression (Y) in relation to R and B was obtained, Figure 9, and a model in the form of isoquants, Figure 10.

$$Y_{(R,B)} = ax^2 + by^2 + cx + dy + exy + f \quad (6)$$

where:

$Y_{(R,B)}$ – wheat production in relation to R and B; x – R spectral values; y – B spectral values; a, b, c, d, e, f – coefficients of the equation (6); a = -0.15562396; b = -0.17124354; c = 56.95051393; d = 54.21621582; e = -0.31153661; f = 0

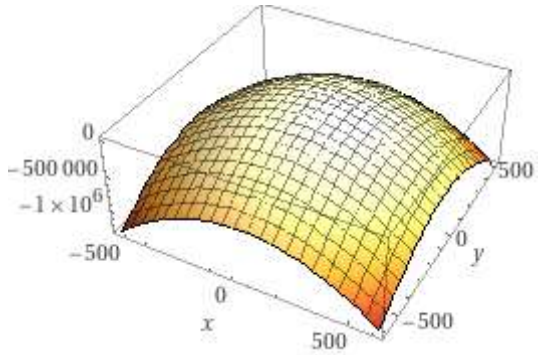

Fig. 9. The 3D graphic distribution of production (Y) in relation to the spectral values R (x-axis) and B (y-axis), Dacic cultivar
Source: Original graph based on recorded and calculated data.

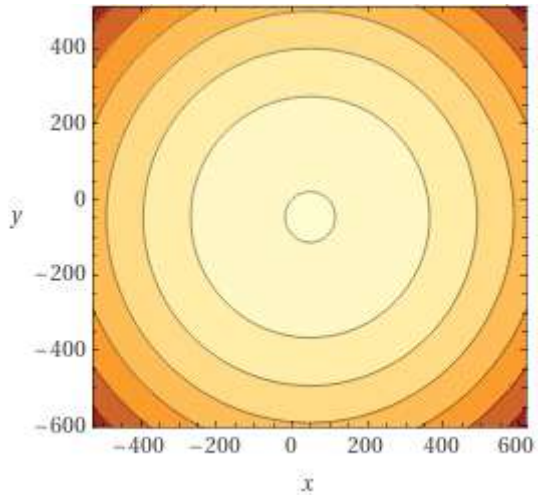

Fig. 10. The graphical distribution in the form of isoquants of the production (Y) in relation to the spectral values R (x-axis) and B (y-axis), Dacic cultivar
Source: Original graph based on recorded and calculated data.

For high precision, up to 16 decimals for the equation (6) coefficients were used.

Based on the trials distribution in the PCA diagram and in the CA dendrogram, 14 trials were selected for Training & model construction (Tmc), and four trials were used for Testing & model validation (Tmv), Table 1. For Testing and model validation (Tmv), trials T2 and T7 were used, with a distinct / independent position in relation to RGB as biplot color parameters, respectively which were integrated into the C1 cluster, and trials T11 and T15, which were positioned in the PCA diagram associated with RGB parameters, and in the CA dendrogram they were included in the C2 cluster.

The regression analysis was used to obtain the wheat production prediction model based on the spectral values of the RGB parameters (Y_{RGB}), obtained from the analysis of aerial images (UAV). Equation (7) was obtained, under statistical safety conditions, according to R2=0.999, p<0.001. For high precision, up to 12 decimal were used in the calculation for the coefficients of equation (7). According to the ANOVA test, the values of the coefficients of equation (7) showed statistical safety, p<0.001 for each equation coefficient (R, G, B).

$$Y_{RGB} = 102.5317R - 122.6898G + 48.0574B \quad (7)$$

where:

Y_{RGB} – Model of production estimation based on RGB values; R, G, B – spectral values

For the testing and validation of the obtained model, the values of the T2, T7, T11 and T15 trials were used, in order to predict wheat production. The estimated production values and the error values compared to the measured production were obtained, Table 4.

Table 4. Values of production predicted based on equation (7), Dacic wheat cultivar

Trial	Trial category	ICH (m)	YP (kg ha^{-1})	Error (kg ha^{-1})
T2	Tmv	2	5,197.829	168.829
T7	Tmv	7	4,922.943	-106.057
T11	Tmv	15	4,985.569	-43.431
T15	Tmv	35	5,034.520	5.520

Source: Original data, obtained by calculation.

Different methods, techniques and models have been developed and used for wheat crop analysis [26] and for agricultural production estimation, in relation to plant species, crop conditions, category of agricultural products, harvest destination, development of agricultural policies, food safety and security [12, 13, 18, 31].

Along with the optimization of agricultural technologies [16, 25], production prediction is useful at the farm level from a logistical perspective, for organizing the process harvesting of agricultural crops, organization and dimensioning of transport, storage spaces, honoring commercial contracts, industrialization etc. [30].

Based on UAV techniques, high levels of prediction in the wheat crop (expressed on the basis of R^2, RMSE, average error) were communicated by different authors in various studies conditions [3, 6, 36].

In the context of the present study, high precision was obtained in the prediction of wheat production based on UAV images, respectively of the RGB color parameters, in relation to the images capture hight (ICH), the absolute error being between 5.520 - 168.829 kg ha^{-1}. The obtained model showed high statistical safety (p<0.001), and the Flowchart diagram of process used can be adapted to different agricultural crops.

CONCLUSIONS

Based on the UAV images taken at different heights (ICH) of the wheat crop, the Dacic cultivar, it was possible to create a flowchart diagram of the process and obtain production prediction models in relation to the values of the RGB color parameters.

Models of the type of polynomial equations were obtained through regression analysis, which described with statistical certainty the variation of RGB color parameters in relation to ICH.

In relation to the PCA and CA analysis, ICH trials were selected for Training & model construction (Tmc), respectively for Testing & model validation (Tmv), and the obtained model facilitated the prediction of production

under conditions of statistical safety under conditions of maximum errors of up to to 168.829 kg ha^{-1}.

Flowchart diagram of process and production prediction models can be adapted for different agricultural crops, in relation to the time and images capture height.

ACKNOWLEDGEMENTS

The authors thank the ARSD Lovrin for facilitating this study.

REFERENCES

[1]Aslan, M.F., Durdu, A., Sabanci, K., Ropelewska, E., Gültekin, S.S., 2022, A comprehensive survey of the recent studies with UAV for precision agriculture in open fields and greenhouses, Appl. Sci., 12(3):1047.

[2]Benami, E., Jin, Z., Carter, M.R., Ghosh, A., Hijmans, R.J., Hobbs, A., Kenduiywo, B., Lobell, D.B., 2021, Uniting remote sensing, crop modelling and economics for agricultural risk management, Nat. Rev. Earth Environ, 2:140-159.

[3]Bian, C., Shi, H., Wu, S., Zhang, K., Wei, M., Zhao, Y., Sun, Y., Zhuang, H., Zhang, X., Chen, S., 2022, Prediction of field-scale wheat yield using machine learning method and multi-spectral UAV data, Remote Sens, 14:1474.

[4]Bouguettaya, A., Zarzour, H., Kechida, A., Taberkit, A.M., 2022, Deep learning techniques to classify agricultural crops through UAV imagery: A review, Neural Comput. Appl., 34:9511-9536.

[5]Constantinescu, C., Herbei, M., Rujescu, C., Sala, F., 2018, Model prediction of chlorophyll and fresh biomass in cereal grasses based on aerial images, AIP Conf. Proc., 1978(1):390003.

[6]Costa, L., McBreen, J., Ampatzidis, Y., Guo, J., Gahrooei, M.R., Babar, M.A., 2022, Using UAV-based hyperspectral imaging and functional regression to assist in predicting grain yield and related traits in wheat under heat-related stress environments for the purpose of stable yielding genotypes, Prec. Agric., 23:622-642.

[7]Czapiewski, S., 2022, Assessment of the applicability of UAV for the creation of digital surface model of a small peatland, Front. Earth Sci., 10:834923.

[8]Hammer, Ø., Harper, D.A.T., Ryan, P.D., 2001, PAST: Paleontological statistics software package for education and data analysis, Palaeontol. Electron., 4(1):1-9.

[9]Han, X., Wei, Z., Chen, H., Zhang, B., Li, Y., Du, T., 2021, Inversion of winter wheat growth parameters and yield under different water treatments based on UAV multispectral remote sensing, Front. Plant Sci., 12:609876.

[10]JASP Team, 2022, JASP (Version 0.16.2) [Computer software].

[11]Jiang, J., Atkinson, P.M., Zhang, J., Lu, R., Zhou, Y., Cao, Q., Tian, Y., Zhu, Y., Cao, W., Liu, X., 2022, Combining fixed-wing UAV multispectral imagery and machine learning to diagnose winter wheat nitrogen status at the farm scale, Eur. J. Agron., 138:126537.

[12]Kheir, A.M.S., Alkharabsheh, H.M., Seleiman, M.F., Al-Saif, A.M., Ammar, K.A., Attia, A., Zoghdan, M.G., Shabana, M.M.A., Aboelsoud, H., Schillaci, C., 2021, Calibration and validation of AQUACROP and APSIM models to optimize wheat yield and water saving in Arid regions, Land, 10:1375.

[13]Kuehne, G., Llewellyn, R., Pannell, D.J., Wilkinson, R., Dolling, P., Ouzman, J., Ewing, M., 2017, Predicting farmer uptake of new agricultural practices: A tool for research, extension and policy, Agric. Syst., 156:115-125.

[14]López, A., Jurado, J.M., Ogayar, C.J., Feito, F.R., 2021, A framework for registering UAV-based imagery for crop-tracking in Precision Agriculture, Int. J. Appl. Earth Obs. Geoinf., 97:102274.

[15]Lu, N., Zhou, J., Han, Z., Li, D., Cao, Q., Yao, X., Tian, Y., Zhu, Y., Cao, W., Cheng, T., 2019, Improved estimation of aboveground biomass in wheat from RGB imagery and point cloud data acquired with a low-cost unmanned aerial vehicle system, Plant Methods, 15:17.

[16]Manos, B., Chatzinikolaou, P., Kiomourtzi, F., 2013, Sustainable optimization of agricultural production, APCBEE Proceedia, 5:410-415.

[17]Meier, U., 2001, Growth stages of mono-and dicotyledonous plants e BBCH monograph, Federal Biological Research Centre for Agriculture and Forestry, 158 pp.

[18]Muruganantham, P., Wibowo, S., Grandhi, S., Samrat, N.H., Islam, N., 2022, A systematic literature review on crop yield prediction with deep learning and remote sensing, Remote Sens., 14:1990.

[19]Noor, N.M., Abdullah, A., Hashim, M., 2018, Remote sensing UAV/Drones and its applications for urban areas: A review, IOP Conf. Ser. Earth Environ. Sci., 169:012003.

[20]Pandey, U.S., Pratihast, A.K., Aryal, J., Kayastha, R.B., 2020, A review on drone-based data solutions for cereal crops, Drones, 4(3):41.

[21]Peprah, C.O., Yamashita, M., Yamaguchi, T., Sekino, R., Takano, K., Katsura, K., 2021, Spatio-temporal estimation of biomass growth in rice using canopy surface model from Unmanned Aerial Vehicle images, Remote Sens., 13:2388.

[22]Rahman, M.F.F., Fan, S., Zhang, Y., Chen, L., 2021, A comparative study on application of Unmanned Aerial Vehicle systems in agriculture, Agriculture, 11(1):22.

[23]Rasband, W.S., 1997, Image J. U. S. National Institutes of Health, Bethesda, Maryland, USA, pp. 1997-2014.

[24]Rejeb, A., Abdollahi, A., Rejeb, K., Treiblmaier, H., 2022, Drones in agriculture: A review and bibliometric analysis, Comput. Electron. Agric., 198:107017.

[25]Roy, P.C., Guber, A., Abouali, M., Nejadhashemi, A.P., Deb, K., Smucker, A.J.M., 2019, Crop yield simulation optimization using precision irrigation and subsurface water retention technology, Environ. Model. Soft., 119:433-444.
[26]Sala, F., Popescu, C.A., Herbei, M.V., Rujescu, C., 2020, Model of color parameters variation and correction in relation to "Time-View" image acquisition effects in wheat crop, Sustainability, 12(6):2470.
[27]Singh, A.P., Yerudkar, A., Mariani, V., Iannelli, L., Glielmo, L., 2022, A bibliometric review of the use of Unmanned Aerial Vehicles in precision agriculture and precision viticulture for sensing applications, Remote Sens., 14:1604.
[28]Stöcker, C., Bennett, R., Koeva, M., Nex, F., Zevenbergen, J., 2022, Scaling up UAVs for land administration: Towards the plateau of productivity, Land Use Policy, 114:105930.
[29]Sweet, D.D., Tirado, S.B., Springer, N.M., Hirsch, C.N., Hirsch, C.D., 2022, Opportunities and challanges in phenotyping row crops using drone-based RGB imaging, Plant Phenome J., 5:e20044.
[30]Taşkıner, T., Bilgen, B., 2021, Optimization models for harvest and production planning in agri-food supply chain: A systematic review, Logistics, 5(3):52.
[31]Van Klompenburg, T., Kassahun, A., Catal, C., 2020, Crop yield prediction using machine learning: A systematic literature review, Comput. Electron. Agric., 177:105709.
[32]Villareal, M., Tongco, A., Maja, J., 2020, Winter wheat crop height estimation using small Unmanned Aerial System (sUAS), Agric. Sci., 11:355-368.
[33]Wolfram Research, Inc., Mathematica, Version 12.1, Champaign, IL (2020).
[34]Wu, S., Deng, L., Guo, L., Wu, Y., 2022, Wheat leaf area index prediction using data fusion based on high-resolution unmanned aerial vehicle imagery, Plant Methods, 18:68.
[35]Yang, B., Zhu, Y., Zhou, S., 2021, Accurate wheat lodging extraction from multi-channel UAV images using a Lightweight Network Model, Sensors, 21(20):6826.
[36]Zeng, L., Peng, G., Meng, R., Man, J., Li, W., Xu, B., Lv, Z., Sun, R., 2021, Wheat yield prediction based on Unmanned Aerial Vehicles-collected Red–Green–Blue imagery, Remote Sens., 13(15):2937.
[37]Zhou, Y., Lao, C., Yang, Y., Zhang, Z., Chen, H., Chen, Y., Chen, J., Ning, J., Yang, N., 2021a, Diagnosis of winter-wheat water stress based on UAV-borne multispectral image texture and vegetation indices, Agric. Water Manag., 256:107076.
[38]Zhou, X., Kono, Y., Win, A., Matsui, T., Tanaka, T.S.T., 2021b, Predicting within-field variability in grain yield and protein content of winter wheat using UAV-based multispectral imagery and machine learning approaches, Plant Prod. Sci., 24(2):137-151.